Effects of Zn Doped TiO_2 on the Performance of Perovskite Solar Cells

D. J. Reddy[1], I. J. Larzarus[2*]
[1]Faculty of Engineering and the Built Environment, Department of Electrical Power Engineering, Durban University of Technology, Durban, South Africa
[2]Faculty of Engineering and the Built Environment, Department of Physics, Durban University of Technology, Durban, South Africa
[*]corresponding author's email: lazarusi@dut.ac.za

Abstract – *The work focuses on the effects of Zn-doped* TiO_2 *as the Electron Transport Layer in MAPbI3 based Perovskite Solar Cells with a carbon-based back electrode fabricated under controlled ambient conditions. Varying molar percentages of Zn-doped* TiO_2 *of 0, 0.5, 1, 2, and 5 mol% were successfully incorporated into the* TiO_2 *crystal structure using the sol-gel technique. Characterization through X-ray diffraction and Energy Dispersive X-ray spectroscopy confirmed the incorporation of Zn ions. The crystallite size ranged from 19.99 to 7.1 nm, depending on the Zn ion doping concentration. Fourier Transform Infrared spectroscopy verified the presence of the anatase phase of Zn-doped* TiO_2 *at wavenumber 438* cm^{-1}*. Scanning Electron Microscope images exhibited fairly smooth and uniform surface coverage for the Zn-doped* TiO_2 *layers. The Rq values for surface roughness showed a decrease from 26.85 nm for undoped* TiO_2 *to 23.4 nm for the 5 mol% Zn-doped* TiO_2 *layer. UV-Vis spectroscopy demonstrated low light transmission loss characteristics from 300 to 790 nm, with the 2 mol% Zn-doped* TiO_2 *showing slightly improved light transmission between 550 and 800 nm. The bandgap energy of undoped and Zn-doped* TiO_2 *ranged from 3.53 to 3.38 eV. An optimum power conversion efficiency of 5.67% was achieved with a 2 mol% dopant concentration. However, increasing the Zn dopant to 5 mol% led to a slight deterioration in the PCE. According to the optimized ETL processing for the PSC, the Jsc increased from 12.2185* mA/cm^2 *to 12.25594* mA/cm^2*, the Voc increased slightly from 0.90569 V to 0.9231 V, and the PCE from 5.199% to 5.67%.*

Keywords*: Conduction Band (CB), Perovskite Solar Cells (PSC), Power Conversion Efficiency (PCE), Titanium dioxide, Zn doped*

Article History
Received 18 January 2024
Received in revised form 17 April 2024
Accepted 26 April 2024

I. Introduction

Perovskite, which has the general crystal structure ABX_3, is the absorber component used in perovskite solar cells (PSCs). The perovskite form of ABX_3 with methyl ammonium (CH_3NH_3) as (A), metal such as lead (Pb) or tin (Sn) as (B), and a halide bromide (Br_3), iodide (I_3), or chloride (Cl_3) as (X_3) has so far been used to make the most effective PSC devices [1]. Perovskite has the following advantages: a low band gap that permits greater light absorption, a high carrier charge mobility that enables the generated electron and hole to move through the substance with little resistance, and a high diffusion length that inhibits electron-hole pair recombination [2].

Metal oxides such as zinc oxide (ZnO) [3], aluminum oxide (Al_2O_3) [4], tin oxide (SnO_2) [5], and titanium dioxide (TiO_2) have been used as the ETL to improve electron transportation and the PCE. TiO_2 exhibits attractive characteristics such as chemical stability, low cost, and high transport ability [6]. This is attributed to the conduction band (CB) of TiO_2 being lower than the conduction band of the perovskite absorber layer, facilitating the electron transport from the perovskite layer to the TiO_2 layer [6].

For the PSC to function effectively, the energy levels for each layer, as shown in Fig. 1, must be carefully aligned. This is accomplished by having the lowest unoccupied molecular orbital (LUMO) of the ETLs slightly lower than that of the active layers, which provides an electron with a more desirable path to travel.

The same applies to the HTLs HOMO (highest occupied molecular orbital), which must be slightly higher than the active layers HOMO to offer a more attractive path for holes. This is similar for each layer in the cell; each layer must have either a greater HOMO or a lower LUMO in order for the charge carriers' transportation chain to function [7].

Materials are doped to increase charge carrier conductivity by adding an extra molecule to their structure. Doping changes the band structure and trap states of TiO_2, altering important properties such as conduction band energy, charge transport, recombination, and collection [8]. TiO_2 doped with Mg, Nb, Y, Al, and Zr has previously been used in perovskite solar cells. Mg-doped HBL/ ETL has improved V_{OC} because of its strong conduction band and low recombination [9]. Nb doping boosted electron injection and transport, resulting in greater JSC [10], and Y doping improved performance due to increased perovskite loading, resulting in significant increases in JSC and marginally reduced recombination [11]. It has been found that Al-doping reduces the number of oxygen vacancies and the associated deep trap states, lowering recombination and increasing film conductivity. As a result, J_{SC} increased overall [12]. Doping TiO_2 with Zr^{4+} reduced hysteresis while pushing the CB upward and reducing recombination, resulting in an increase in VOC [13, 14].

These results suggest that doping is important in lowering surface trap states, reducing hysteresis, and enhancing current density. Overall, these results suggest that TiO_2 doping and co-doping are expected to play an important role in lowering surface trap states, reducing hysteresis, enhancing current density, and improving PSC efficiencies. Doping causes the CB to shift, hence increasing charge transfer and decreasing recombination. Additionally, it has the ability to increase perovskite loading, lengthen device lifetimes, and play a vital role in reducing hysteresis [15].

Recent advancements in perovskite solar cell technology have highlighted the need for improved electron transport layers. This research focuses on the use of Zn-doped TiO_2 compact layer with variable doping concentrations of 0, 0.5, 1, 2 and 5 mol % as an electron transport layer. A number of n-i-p structure perovskite solar cells were developed. The Zn-doped TiO_2 compact layers' structural, morphological and optical properties are also analyzed and discussed. The photovoltaic properties of perovskite solar cells with various Zn-doped TiO_2 compact layers as electron transport layers are discussed. The research addresses the need to improve the electron compact layer, which will aid in developing future highly efficient perovskite solar cells using carbon-based electrodes.

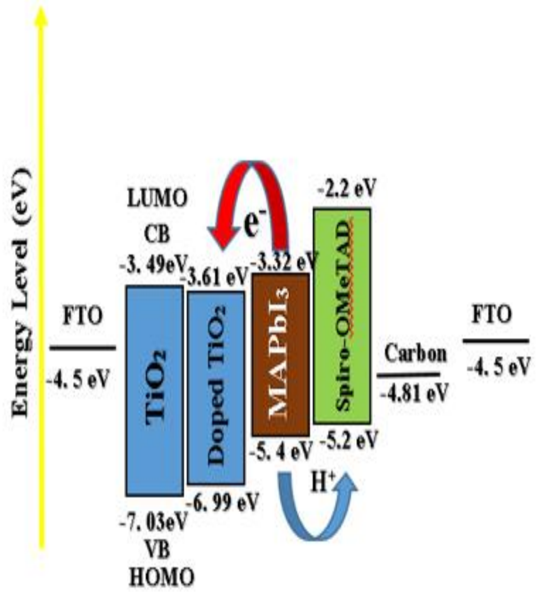

Fig. 1. Energy level band diagram

II. Materials

All chemicals used in the fabrication of the ETL, perovskite and HTL are listed in Table I and were purchased from Sigma-Aldrich Co.

TABLE I
LIST OF CHEMICALS

Layer	Chemicals
Electron Transport Layer Zn-doped TiO_2	Titanium isopropoxide (TTIP), ethanol (EtOH, super dehydrated,), hydrochloric acid (HCL), zinc chloride
Absorber Layer Perovskite	Methyl ammonium iodide (MAI, 99%), Lead (II) Iodide ($PbI_{2,}$ 99.9%), dimethylformamide (DMF, super hydrated), dimethyl-sulfoxide (DMSO, super hydrated), di-ethyl Ether
Hole Transport Layer Spiro- OMeTAD	2, 2', 7, 7'-Tetrakis (N, N-di-p-methoxyphenylamino)-9, 9'-Spirobifluorene (Spiro- OMeTAD powder), 4- Tert – Butylpyridine (TBP, 96%), Bis (triflouromethane sulfonimide lithium salt (LiTFSI), chlorobenzene

III. Device Fabrication

A. Substrate Preparation

Fluorine-doped tin oxide (FTO) coated glass substrates of 25 mm x 25 mm with a thin film thickness of 100 nm and sheet resistance of 8.3 Ω were cleaned in a beaker containing detergent and deionized water. Each substrate was then rinsed in an acetone before being placed in the ultrasonic cleaner. The substrates were then immersed for 20 minutes at 80 °C in the ultrasonic cleaner containing ethanol. The substrates were removed and placed into a beaker containing deionized water before being placed on a hotplate at 60 °C for 10 minutes or until totally dry. The substrates were then placed for 20 minutes in an Ultra Violet Ozone (UVO) cleaner to break down organic surface impurities and provide an ultra-clean surface for the deposition of the ETL layer.

B. Zn – doped ETL layer preparation and deposition

In a volumetric flask, 40 ml di-ionized water was combined with 7.29 ml HCL and mixed for 3 minutes before adding additional de-ionized water up to 100 ml to obtain a 2M HCL stock solution. To prepare the 0.22 M TiO_2 precursor solution with Zn doping of 0.5, 1, 2, 5 mol%, the required amount of Zinc Chloride was added to 14.29 ml ethanol and stirred vigorously at 6000 rpm for 30 minutes, then 0.28 ml of the 2M HCL stock solution was slowly added and stirred vigorously at 6000 rpm for an additional 30 minutes, after which 1 ml of TTIP was slowly added and stirred for 2 hours. The resulting solution was then filtered using a 0.45 µm Teflon filter before spin coating to ensure the removal of small particles to obtain a smooth and uniform surface coverage. The FTO substrates were then pre-heated to 60 °C before dynamically spin coating 300 µl of the Zn-doped ELT precursor solution at 1000 rpm for 15 seconds and annealed on a ceramic digital hotplate at 550 °C for 30 minutes to form the Zn-doped ETL thin film layer. This layer was then UVO treated for 15 minutes prior to the deposition of the methyl ammonium lead iodide precursor solution.

C. Perovskite layer preparation and deposition

To prepare the perovskite precursor solution, 0.16 g of methyl ammonium iodide and 0.46 g of lead iodide were added to 0.08 ml of dimethyl sulfoxide (DMSO) and 0.6 ml of dimethylformamide (DMF) and magnetically stirred at 3000 rpm for 24 hours. Then 250 µl of the perovskite solution was statically spin-coated at 5000 rpm for 15 seconds, with 350 µl of di-ethyl ether slowly dripped from a distance of about 2 cm from the revolving substrate during the final 5 seconds. To develop the dark brown and semitransparent perovskite layer, the coated surface was placed on a digital hotplate at 65 °C for 1 minute, then slowly ramped up to 100 °C and annealed for 2 minutes. This was then placed in a vacuum desiccator for 3 hours before deposition of the hole transport layer to minimize exposure to oxygen and humidity.

D. HTL preparation and deposition

The hole transport layer was prepared by dissolving 0.52 g of LiTFSI in 1 ml acetonitrile and stirring vigorously for 10 minutes to form the LiTFSI stock solution. Then, 0.07 g of Spiro-OMeTAD powder was added to 1 ml chlorobenzene and stirred vigorously for 10 minutes to form the Spiro-OMeTAD solution. After this 0.03 ml of tBP and 0. 02 ml of the LiTFSI solution was added to the Spiro-OMeTAD solution and stirred for 30 minutes. Thereafter, 200 µl was dynamically spin-coated at 1000 rpm for 15 seconds and placed in a vacuum desiccator overnight before applying ~8 mg of activated carbon powder and FTO to form a metal-free back conductive electrode.

E. Synthesis Zn- doped TiO_2 nanoparticles

To synthesize the zinc-doped TiO_2 nanoparticles, the Zn-doped ETL precursor solution was aged for 72 days to form a clear and transparent gel. The gel was then dried for 12 hours at 80 °C in a hot air dryer to obtain dry TiO_2 powder. After drying, the TiO_2 powder is heated for 30 minutes at 550 °C in a furnace to produce anatase TiO_2 nanoparticles for FTIR, XRD, and TEM investigation.

IV. Characterization Equipment

The functional groups were identified using an Agilent Cary 630 ATR-FTIR with a diamond crystal operating between 400 and 4000 cm^{-1}. The X-ray diffractometer, type D8 Advanc, manufactured by M/s Bruker AXS, Germany was used to determine the Zn doped- TiO_2 crystal structure and orientation. The surface morphological qualities and elemental percentage concentration were determined using a Zeiss scanning electron microscope at 40 kV and 40 mA. The size of the particles was determined using a Transmission Electron Microscope and Image J software. The Agilent Cary 60 UV-Vis-NIR spectrometer was used to measure the optical characteristics. The photoluminescence intensity measurements were carried out using the Perkin Elmer Lambda 35 UV/ Vis spectrometer. The TAUC plot with a direct bandgap power factor was used to calculate bandgaps. The photovoltaic characteristics were measured using a Keithley 2460 source measurement instrument and an AM 1.5 (1000 W/ m^2) LED light source.

V. Results and Discussion

A. X-Ray Diffraction

For nanoparticles, XRD is typically employed to identify the crystal phase structure and estimate crystallite size and crystallinity [16]-[17]. The XRD diffraction patterns of zinc-doped titanium dioxide powder samples are shown in Fig. 2. Fig. 2 shows the XRD patterns of Zn-TiO_2 powder samples doped with 0.5%, 1%, 2%, and 5% Zn. The XRD peaks at $2\theta = 25.1°$ (101), 37.8° (004), 47.1° (200), 53.4° (105), 54.5° (211), and 61.8° (204) are typically characterized as the typical diffraction peaks of the anatase crystal phase of tetragonal titanium dioxide structure (JCPDS No. 21-1272) with excellent surface performance[18]. All Zn-TiO_2 samples show a pure anatase phase with no rutile phase or zinc ions. Due to the low Zn content, no additional diffraction peaks associated to ZnO develop even at the greatest Zn dopant concentration (5 mol %).

Fig. 3 shows the EDX spectroscopy confirming the weight percentage composition of Zn-doped TiO_2. Furthermore, Fig 2 shows that the sample doped with 0.5 % Zn was largely amorphous, and the half-width of the peak (101) plane increases slightly as the doped Zn amount increases, indicating that the degree of crystallinity of samples as well as crystallite size decreases while the surface defect content increases. This could be attributed to the slight inhibition of TiO_2 crystal formation by Zn doping during the heat treatment process [19]. Furthermore, the peak intensity of the (101) plane increases with increasing Zn doping up to 5 %, which can be attributed to the influence of Zn^{2+} into the TiO_2 lattice structure, as previously found by Arunachalam et al. [20]. Additionally, with Zn ion insertion, XRD patterns exhibited a slight shift to lower angles because the ionic radius of Zn^{2+} (i.e., 0.074 nm) is greater than that of Ti^{4+} (i.e., 0.061 nm). It suggests that Zn^{2+} may enter the TiO_2 lattice or interstitial site [21]. The phase composition of Zn-doped TiO_2 films is shown to be dependent on dopant concentration. The crystallite size (D) for the samples containing 1%, 2%, and 5% Zn was approximately 12.7, 10.8, and 7.1 nm, respectively, as determined by the Debye Scherrer's formula in (1) [22] from the half width (β) of the peak at $2\theta = 25.1°$.

$$D = k\lambda\,(\beta \cos \theta) \tag{1}$$

where k is the shape factor (0.9), D is the average crystallite size, β is the half-width of the measured diffraction peak, θ is the diffraction angle, and λ is the X-ray wavelength (0.154 nm).

B. Fourier Transform Infrared

The FTIR measurement of undoped and Zn doped TiO_2 nanoparticles calcined at 550° C was performed using an Agilent Cary 60. The absence of O-H hydroxyl groups in the wavenumber range 3100-3600 cm^{-1} presented in Fig. 4 can be explained by the high calcination temperature of 550 °C and the elimination of hydroxyl groups. The interactions of the hydroxyl groups with the NH_4 and CH_3 in the perovskite could reduce the performance of the PSC, resulting in the breakdown of $CH_3NH_3PbI_3$ into PbI_2 and CH_3NH_3I [23]. Sharp peaks related to O-Ti-O bonding between 528 and 408 cm^{-1} indicate that the thin layer is crystalline. The prominent peak at 438 cm^{-1} is typical of Zn doped- TiO_2 anatase phase nanoparticles [19]-[25].

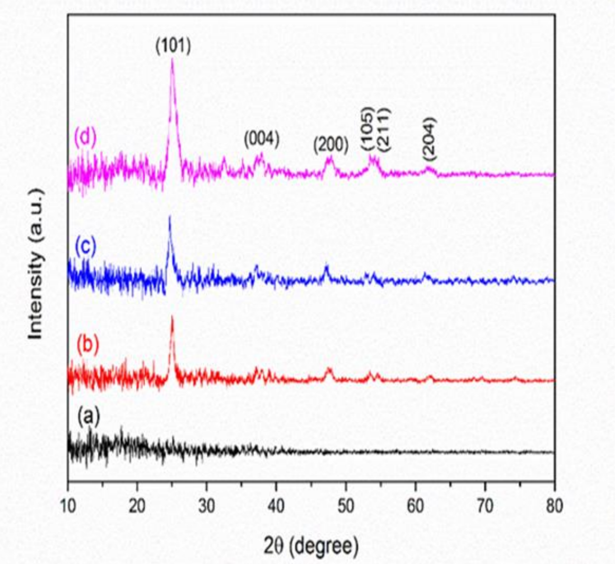

Fig. 2. XRD patterns of Zn-TiO_2 powder samples doped with (a) 0.5%, (b) 1%, (c) 2%, and (d) 5%

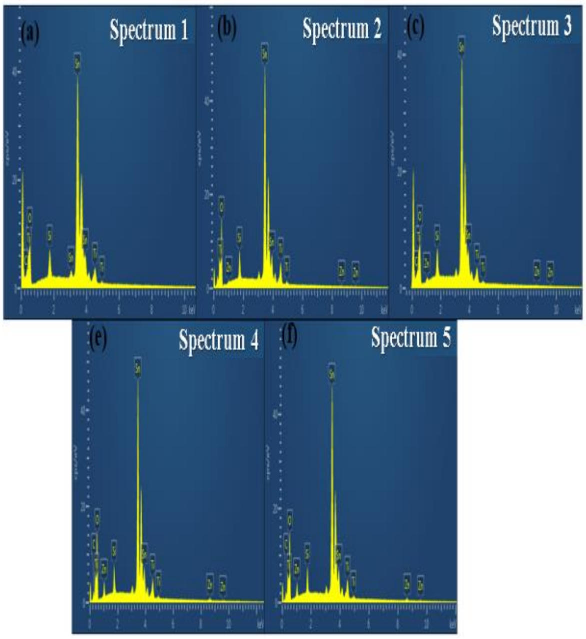

Fig. 3. Elemental weight percentage compositions of (a) undoped TiO_2 (b) 0.5 mol% (c) 1 mol% (d) 2 mol% (e) 5 mol%

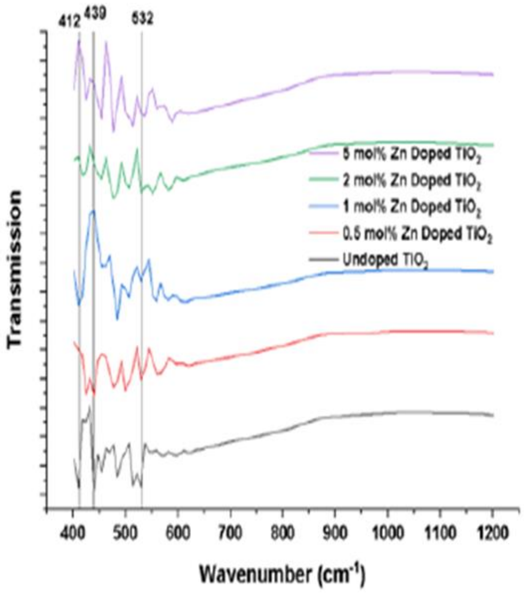

Fig. 4. FTIR results of planar Zn doped TiO_2 nano particles annealed at 550 °C

C. Scanning Electron Microscope

SEM was used to examine the morphology of the TiO_2 and Zn-doped TiO_2 nanoparticles after annealing at 550° C for 30 minutes. The top view of the SEM images of the TiO_2 and Zn-doped TiO_2 layers is shown in Fig. 5. Fig. 5(a) shows a porous and fairly uniform surface covering with no discernible pinholes created on the surface for the undoped TiO_2 sample. The Zn-doped TiO_2 nanoparticles on the surface exhibit an irregular morphology and a conical shape as shown if Fig. 5(b)-(e). According to the SEM images, TiO_2 nanoparticle instability results in agglomeration, which causes the particles to bond. The aggregation of the nanoparticles is further illustrated by the SEM images showing the formation of clusters which appears to reduce upon increasing Zn doping concentration. This could also be attributed to the decrease in crystallite size upon increasing Zn doping observed by the XRD characterization. The surface profiles and Root Mean Square (Rq) values shown in Fig. 6 indicates the surface roughness values of the samples. Fig. 6(a) shows the highest surface roughness of 26.85 nm for the undoped TiO_2 sample and lowest surface roughness of 23.4 nm for the 5 mol% Zn doped TiO_2 layer is shown Fig. 6(e).

It can be seen in Fig. 6(f) that the surface roughness rate decreased gradually from 26.85 to 23.4 nm with increasing Zn doping concentration from 0 to 5 mol %. The reason for the decrease in surface roughness and smoother surfaces could be due to less aggregation due to the dispersion of TiO_2 upon Zn doping [26]-[28]. The surface smoothness of Zn doped TiO_2 compact layer has a critical role in the electron transport behaviour by providing an improved surface interface for the deposition and annealing of the perovskite layer which is critical for improving the performance of PSC [29].

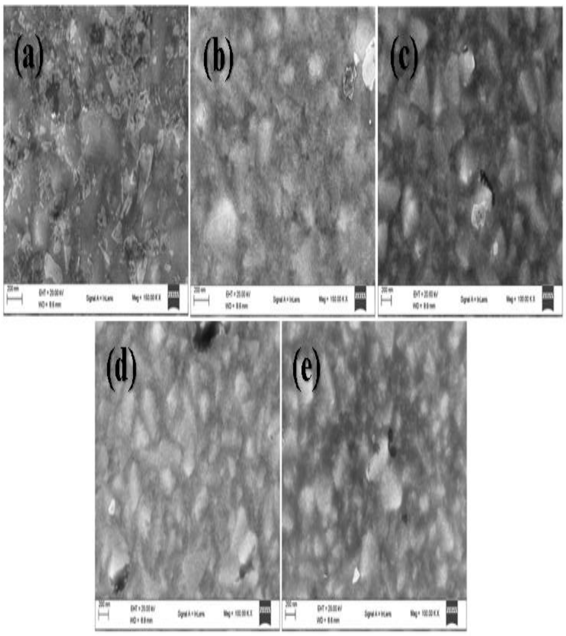

Fig. 5. SEM images of the (a) undoped TiO_2 (b) 0.5 mol% Zn (c) 1 mol% (d) 2 mol% (e) 5 mol%

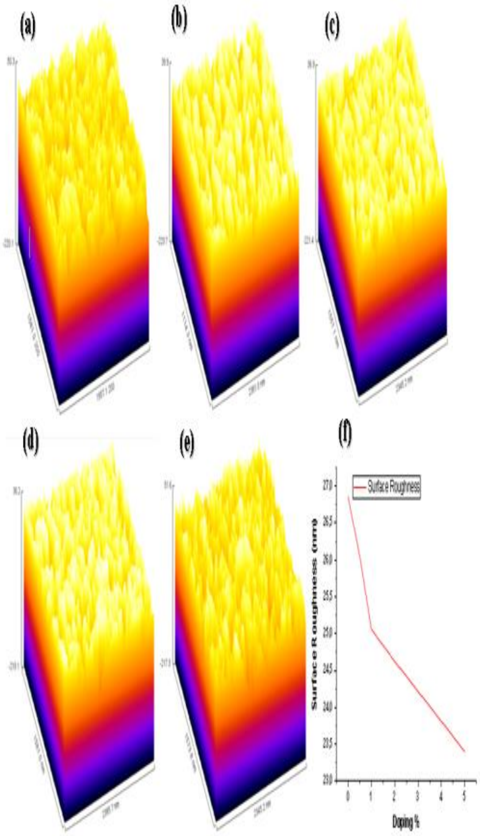

Fig. 6. Surface roughness of (a) undoped TiO_2 (b) 0.5 mol% (c) 1 mol% (d) 2 mol% (e) 5 mol% (f) surface roughness vs doping %

D. Transmission Electron Microscope

The synthesized nano particles size and shape was further investigated by TEM and are shown in Fig. 7 which shows the morphology and size distribution of the TiO_2 nanoparticles ranging from 15 to 20 nm. The Zn doped TiO_2 exhibits a homogenous spherical morphology. The TEM results show an increase in the particle size from 15.91 nm for undoped TiO_2 to 20.31 nm for 5 mol % Zn doped TiO_2, this could be attributed to the incorporation of Zn ions into the TiO_2 lattice structure [30]-[31]. The larger particle size reduces the bandgap and recombination sites in the ETL layer as the space between the valence and conduction bands narrows and electron – hole pairs are further apart and effect of the coulomb interaction between them is reduced [32]-[33]. This is confirmed by the TAUC plot in Fig. 8, which shows bandgap narrowing as the particle size increases from 0 to 5 mol % Zn doping.

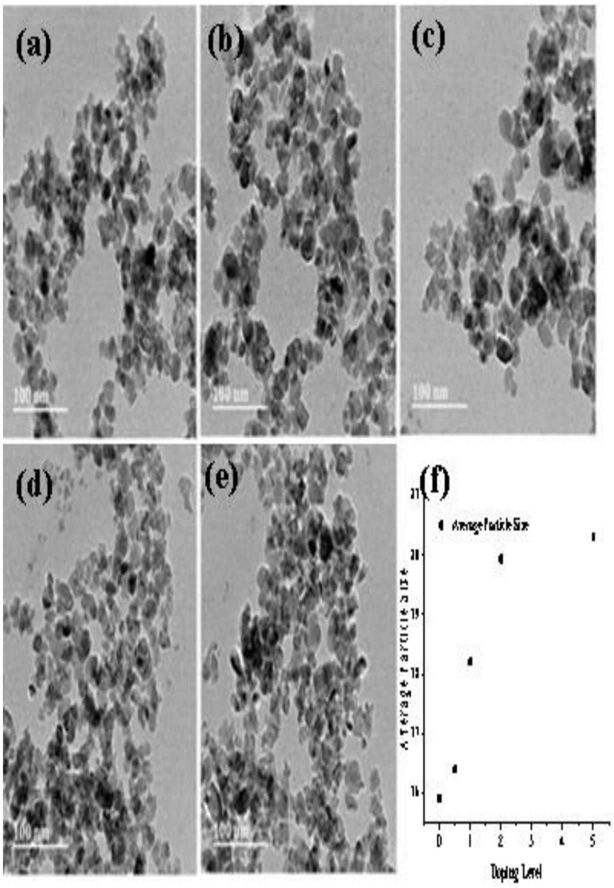

Fig. 7. TEM images of (a) undoped TiO_2 (b) 0.5 mol% (c) 1 mol% (d) 2 mol% (e) 5 mol% (f) average particle size vs doping %

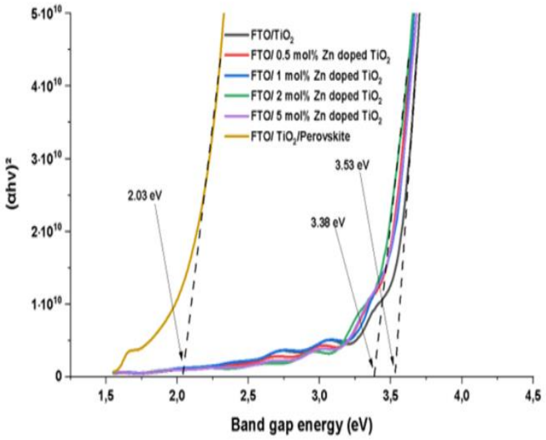

Fig. 8 Tauc Plot

E. Energy Dispersive X-Ray

Energy dispersive X ray spectrometry analysis of TiO_2 thin films was performed using a Zeiss scanning electron microscope to determine and identify the elemental composition and concentrations of the FTO\Zn-TiO_2 layers and is shown below in Table II. It can be seen that the wt % of Zn increases from 0 to 1.08 as the molar percentage concentration increases from 0 to 5 mol %.

Fig. 3 (a)-(e) previously shows peaks for Ti, O, Zn, Sn and Si. The spectra include small peaks of carbon which may be due to the carbon tape fixed on the SEM stub during characterization, no other impurities are seen. Overall, the EDX spectra indicates crystalline synthesis of Zn doped TiO_2 nanoparticles.

TABLE II
ELEMENTAL COMPOSITION AND CONCENTRATIONS OF THE FTO\ ZN- TIO2 LAYERS

Sample	C	O	Si	Ti	Zn	Sn
Spectrum 1 Undoped TiO_2	0	27.2	2.75	3.05	0	66.9
Spectrum 2 0.5 mol%-Zn Doped TiO_2	2.11	29.1	2.33	3.95	0.29	62.3
Spectrum 3 1 mol%-Zn Doped TiO_2	2.56	27.1	2.50	3.85	0.38	63.5
Spectrum 4 2 mol%-Zn Doped TiO_2	2.02	27.9	2.79	3.82	0.49	62.9
Spectrum 5 5 mol%-Zn Doped TiO_2	1.74	28.8	2.22	3.24	1.08	62.8

F. UV-Vis Spectroscopy

The Cary 60 UV-Vis was used to collect UV-Vis transmission and absorption spectra. The UV-Vis transmission spectra of various TiO_2 and Zn-doped TiO_2 thin films coated on FTO substrates are shown in Fig. 9. The transmission intensity of the Zn doped TiO_2 thin film samples decreased between 380 and 550 nm when compared to the undoped TiO_2 sample; between 550 and 800 nm a slight increase is observed for the 2 mol % Zn doped sample, either than that, there is no discernible variation in transmission intensity. The transmission spectra of between 65 – 70 % over this region show a slight light loss when compared to the transmittance of the FTO substrate of between 70 – 80 %. The slight increase in optical transmission exhibited by the 2 mol % Zn doped TiO_2 could be due to a decrease in surface roughness by the incorporation of Zn ion into the TiO_2 lattice structure [34]-[35], this slight improvement in optical transmission will directly increase the light absorption of the perovskite film.

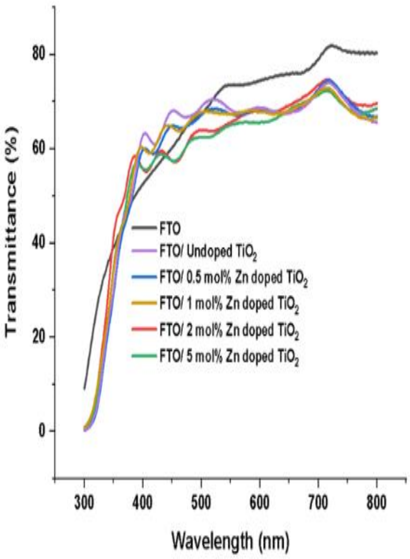

Fig. 9. Transmission spectra of undoped and Zn-doped TiO_2

The absorption spectra of TiO_2 and Zn-doped TiO_2 samples are shown in Fig 10, as can be seen from the results there is a clear improvement in the optical absorption from a range of 300 nm to 790 nm with the introduction of Zn ions into TiO_2, this also has a direct influence on the bandgap of the TiO_2 and the Zn doped TiO_2 layers and is shown in Fig. 8 utilizing the TAUC plot.

The band gap of the undoped TiO_2, Zn doped TiO_2, and the perovskite layer was determined by plotting $(a/hv)^2$ as a function of photon energy and extrapolating the linear region of the absorption curve as shown in Fig. 8. The bandgap of the perovskite layer was determined to be 2.03 eV. The bandgaps of undoped TiO_2 and 0.5, 1, 2, 5 mol % Zn doped TiO_2 are respectively 3.53, 3.48, 3.45, 3.38, and 3.41 eV. As the mol% Zn doping concentration increased from 0 % to 5 %, the band gap gradually decreased from 3.53 eV for the undoped TiO_2 down to 3.38 eV for 2 mol%, then increased by 0.03 eV for the 5 mol% when compared to 2 mol%. By increasing Zn doping concentration, the band gap of Zn-doped TiO_2 compact layers decreased and introduced a new band in the TiO_2 bandgap. Previous results indicate that bandgap narrowing can shift the Fermi energy level up and lower the position of the conduction band, which can improve electron injection from the perovskite layer to the Zn-doped TiO_2 compact layer [36].

G. Photoluminescence

To gain insight into the charge transfer kinetics within the TiO_2 and Zn-doped TiO_2 thin films, photoluminescence intensity measurements recorded at room temperature (300 K) was done using the Perkin Elmer Lambda 35 UV/Vis spectrometer at an excitation wavelength of 525 nm.

The excitation wavelength of 525 nm produced a photoluminescence peak at 735 nm (1.69 eV) corresponding closely to the bandgap of the perovskite film. The peak position is slightly lower (0.37 eV) than the bandgap value (2.06 eV) estimated from the Tauc plot but relatively close to the bandgap value of 1.6 eV reported by Kong et al for the tetragonal structure of $CH_3NH_3PbI_3$ [37].

According to the corresponding shape on the PL spectra for the undoped and doped TiO_2 films, Zn doping does not introduce additional PL signals. The broad photoluminescence peak observed at 735 nm is a result of the radiative recombination of electrons and holes near the band edges [38]. This depicts the direct bandgap nature of the $CH_3NH_3PbI_3$ film.

In materials with a direct bandgap, the recombination of charge carriers leads to the emission of photons and in this case, it occurs at 735 nm. Additionally, Fig. 10 shows a decrease in PL intensity from the undoped TiO_2 to the Zn doped TiO_2, with 2 mol% and 5 mol% Zn doped TiO_2 showing the strongest PL quenching indicating electrons can be effectively transferred to the perovskite layer to TiO_2 thus resulting in faster charge transfer kinetics and less recombination. The low emission intensities of the Zn-doped TiO_2 films confirm that Zn doping can reduce electron-hole recombination reactions.

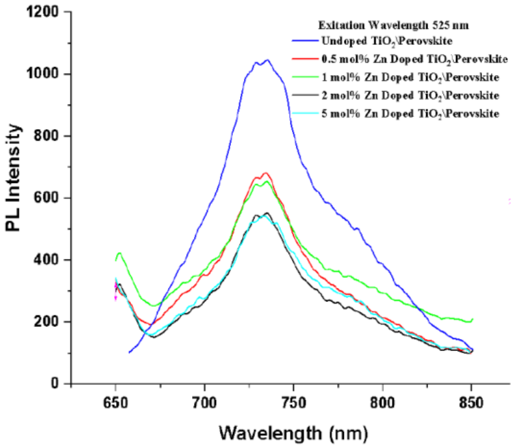

Fig. 10. Photoluminescence spectra of undoped and Zn doped TiO_2

H. PSC Performance

The J-V curves and best performance of the various PSCs developed are shown in Fig. 11. The open circuit voltage slightly improved from 0.90569 V to 0.92774 V when the Zn doping concentration increased from 0 up to 2 mol%, possibly due to the lower conduction band position. Adding Zn ions into the TiO_2 lattice structure raises the CB toward the absorber's LUMO level and enables electron injection from the absorber into the compact layer. When compared to undoped TiO_2, the lower conduction band of Zn-doped TiO_2 improves electron injection from the perovskite to the ETL layer and electron transport rate. Due to bandgap narrowing and improved charge transport, the J_{SC} increased from 12.21851 mA/ cm^2 to 12.25594 mA/cm^2 when Zn doping concentration increased from 0 to 2 mol%.

The PCE of the perovskite solar cell with undoped TiO_2 has a PCE of 5.199 %. As Zn doping concentrations were increased to 2 mol%, the PCE increased to 5.675 % and FF from 48.05 to 49.4823. The PSC with 5 mol% Zn doped TiO_2 has a slightly lower V_{OC}, J_{SC}, FF and PCE. The PCE decreased slightly to 5.5648% compared to 2 mol% Zn-doped TiO_2. A possible reason for the reduction in the efficiency of cells with a doping level of 5 mol% is that this doping level moves the CB of the ETL by ~0.03 eV upward. The electron injection from the absorber layer toward the ETL may be made easier by the proximity of the CB of the ETL to the LUMO of the absorber layer. When the CB goes higher, it moves away from the CB of the FTO layer. As a result, it would raise the recombination rate within the ETL while decreasing electron injection from the CB of the ETL to the CB of the FTO layer [39]. Additionally, the efficiencies are lower than reported values because the PSC performance could have been affected by the humidity under the ambient conditions of fabrication and characterization including the instability of the single cation of perovskite $CH_3NH_3PbI_3$.

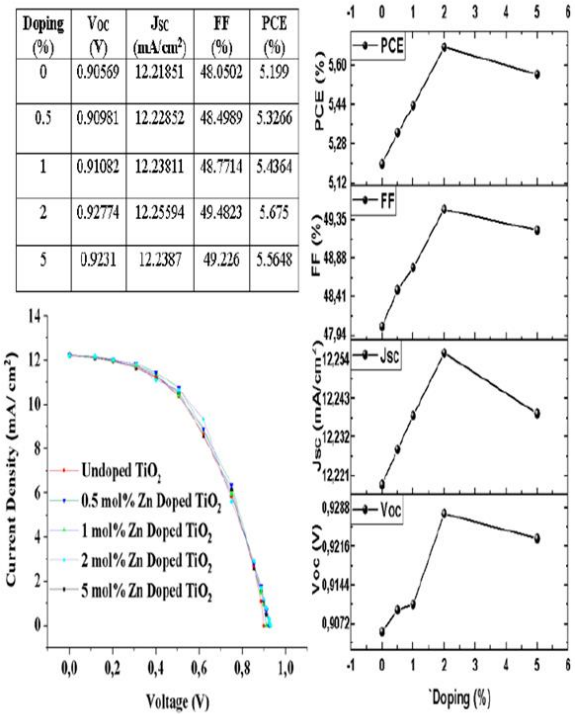

Doping (%)	Voc (V)	Jsc (mA/cm^2)	FF (%)	PCE (%)
0	0.90569	12.21851	48.0502	5.199
0.5	0.90981	12.22852	48.4989	5.3266
1	0.91082	12.23811	48.7714	5.4364
2	0.92774	12.25594	49.4823	5.675
5	0.9231	12.2387	49.226	5.5648

Fig. 11. PV characteristics of Zn-TiO_2 PSC's

VI. Conclusion

Finally, using the sol-gel technique followed by thermal annealing, several Zn-doped TiO_2 compact layers with variable Zn doping concentrations are successfully produced. The impact of Zn doping concentration on changes in structural, morphological, optical, and performance photovoltaic properties was studied systemically. The data indicates an improvement in surface smoothness, particle morphology, and optical properties and induces band gap narrowing. This correspondingly improves the bandgap alignment with the perovskite absorber layer and the PCE. With a Zn doping concentration of 2 mol%, the structural, morphological, optical, and performance properties are optimum. The *Jsc* of perovskite solar cells increased from 12.2185 mA/cm^2 to 12.25594 mA/cm^2, V_{OC} decreased from 0.90569 to 0.92774 V and the PCE increased from 5.199 % to 5.675 %. Importantly, the Zn-doped TiO_2 PSCs developed under the mentioned controlled conditions allow for reasonable reproducibility and reliability without using an expensive glovebox and thermal evaporation equipment for the back metal contacts.

Further study to investigate the influence of process conditions on the structure of TiO_2 is a good starting point to further improve TiO_2 at an ETL in PSC's.

understanding how defects in the materials are created during fabrication is vital, as this significantly affects the material's properties. Synthesized anatase phase TiO_2 nanoparticles at 550 °C consume high electrical energy during annealing and limit device fabrication to solid substrates. Investigation and optimization into low temperature annealing for TiO_2 will allow annealing onto more flexible substrates such as Polyethylene (PET) and provide a way to develop flexible PSC, allowing for numerous applications. Annealing the TiO_2 thin films at varying temperatures and studying their influence on crystallinity, trap states, conduction band position, elemental composition, and recombination will allow linking of annealing temperature, material composition, and device performance.

Acknowledgments

The authors gratefully acknowledge the financial support from the South African National Research Foundation grant reference TTK200309508592.

Declaration on Conflict of Interest

The authors have no conflict of interest in the publication process of the research article.

Statement on Author contributions

D. J. Reddy's contributions included conception, device fabrication, data collection, analysis and interpretation. I. J. Lazarus's contributions included drafting of the article, critical revision of the article and final approval of the version to be submitted.

References

[1] I. Mesquita, L. Andrade, and A. Mendes, "Perovskite solar cells: Materials, configurations and stability," Renewable and Sustainable Energy Reviews, vol. 82, pp. 2471–2489, Feb. 2018, doi: 10.1016/j.rser.2017.09.011.

[2] J. Bisquert, The Physics of Solar Cells: Perovskites, Organics, and Photovoltaic Fundamentals, 1st ed. Boca Raton, FL : CRC Press, Taylor & Francis Group, [2018]: CRC Press, 2017. doi: 10.1201/b22380.

[3] A. K. Chandiran, M. Abdi-Jalebi, M. Nazeeruddin, and M. Graetzel, "Analysis of Electron Transfer Properties of ZnO and TiO_2 Photoanodes for Dye-Sensitized Solar Cells," *ACS nano*, vol. 8, Feb. 2014, doi: 10.1021/nn405535j.

[4] Y.-N. Zhang, B. Li, L.-Y. Zhang, and L.-W. Yin, "Efficient electron transfer layer based on Al_2O_3 passivated TiO_2 nanorod arrays for high performance evaporation-route deposited $FAPbI_3$ perovskite solar cells," *Solar Energy Materials and Solar Cells*, vol. 170, pp. 187–196, Oct. 2017, doi: 10.1016/j.solmat.2017.05.072.

[5] Z. Cao *et al.*, "Metal Oxides Alternatives for Efficient Electron Transport in Perovskite Solar Cells: Beyond TiO_2 and SnO_2," *Journal of Materials Chemistry A*, vol. 8, Aug. 2020, doi: 10.1039/D0TA07282F.

[6] T. Kim, J. Lim, and S. Song, "Recent Progress and Challenges of Electron Transport Layers in Organic–Inorganic Perovskite Solar Cells," Energies, vol. 13, no. 21, p. 5572, Oct. 2020, doi: 10.3390/en13215572.

[7] N. Marinova, S. Valero and J. L. Delgado, "Organic and perovskite solar cells: Working principles, materials and interfaces," *Journal of Colloid and Interface Science*, vol. 488, pp. 373-389, November 2016.

[8] B. Roose, S. Phathak and U. Steiner, "Doping of TiO_2 for sensitized solar cells," *Royal Society of Chemistry*, 28 April 2015.

[9] J. Wang, M. Qin, H. Tao, W. Ke, Z. Chen, J. Wan, P. Qin, L. Xiong, H. Lei, H. Yu and G. Fang, "Performance enhancement of perovskite solar cells with Mg-doped TiO_2 compact film as the hole-blocking layer," Applied Physics Letters, vol. 106, no. 12, p. 121104, 2015.

[10] G. Yin, J. Ma, H. Jiang, J. Li, D. Yang, F. Gao, H. J. Zeng, Z. Lui and S. Liu, "Enhancing Efficiency and Stability of Perovskite Solar Cells through Nb-Doping of TiO_2 at Low Temperature," *ACS Applied Materials & Interfaces*, vol. 9, 2017.

[11] X. Deng, Y. Wang, Z. Cui, L. Li, and C. Shi, "Y-doping TiO_2 nanorod arrays for efficient perovskite solar cells," *Superlattices and Microstructures*, vol. 117, pp. 283–287, May 2018, doi: 10.1016/j.spmi.2018.03.051.

[12] S. K. Pathak, A. Abate, P. Ruckdeschel, B. Roose, K. C. Godel, Y. Vaynzof, A. Santhala, S.-I. Wantanabe, D. J. Hollman, N. Noel, A. Sepe, U. Weisner, R. Friend, H. J. Snaith and U. Steiner, "Performance and Stability Enhancement of Dye-Sensitized and Perovskite Solar Cells by Al Doping of TiO_2," *Advanced Functional Materials*, vol. 24, no. 38, pp. 6046-6055, 2014.

[13] H. Nagaoka, F. Ma, D. W. deQuilettes, S. M. Vorpahl, M. S. Glaz, A. E. Colbert, M. E. Ziffer and D. S. Ginger, "Zr Incorporation into TiO_2 Electrodes Reduces Hysteresis and Improves Performance in Hybrid Perovskite Solar Cells while Increasing Carrier Lifetimes," Journal of Physical Chemistry Letters, vol. 6, no. 4, pp. 669-675, 2015.

[14] N. H et al., "Zr Incorporation into TiO_2 Electrodes Reduces Hysteresis and Improves Performance in Hybrid Perovskite Solar Cells while Increasing Carrier Lifetimes.," J Phys Chem Lett, vol. 6, no. 4, pp. 669–675, Feb. 2015, doi: 10.1021/jz502694g.

[15] D.-Y. Son et al., "Universal Approach toward Hysteresis-Free Perovskite Solar Cell via Defect Engineering," J. Am. Chem. Soc., vol. 140, no. 4, pp. 1358–1364, Jan. 2018, doi: 10.1021/jacs.7b10430.

[16] Roshanghias, A., G. Sodeifian, A.A. Javidparvar, and S. Tarashi, "Construction of a novel polytetrafluoroethylene-based sealant paste: The effect of polyvinyl butyral (PVB) and nano-alumina on the sealing performance and construction formulations", *Results in Engineering 14*, 2022, pp. 100460.

[17] Bunaciu, A.A., E. Gabriela Udriştioiu, and H.Y. Aboul-Enein, "X-Ray Diffraction: Instrumentation and Applications", *Critical Reviews in Analytical Chemistry 45*(4), 2015, pp. 289–299.

[18] Aware, D. V., and S.S. Jadhav, "Synthesis, characterization and photocatalytic applications of Zn-doped TiO_2 nanoparticles by sol–gel method", Applied *Nanoscience 6*(7), 2016, pp. 965–972.

[19] Chauhan, R., A. Kumar, and R.P. Chaudhary, "Structural and optical characterization of Zn doped TiO_2 nanoparticles prepared by sol–gel method", *Journal of Sol-Gel Science and Technology 61*(3), 2012, pp. 585–591.

[20] Arunachalam, A., S. Dhanapandian, C. Manoharan, and G. Sivakumar, "Physical properties of Zn doped TiO_2 thin films with spray pyrolysis technique and its effects in antibacterial activity", *Spectrochimica Acta Part A: Molecular and Biomolecular Spectroscopy 138*, 2015, pp. 105–112.

[21] Ghanbari Niaki, A.H., A.M. Bakhshayesh, and M.R. Mohammadi, "Double-layer dye-sensitized solar cells based on Zn-doped TiO_2 transparent and light scattering layers: Improving electron injection and light scattering effect", *Solar Energy 103*, 2014, pp. 210–222.

[22] Hajipour, F., S. Asad, M.A. Amoozegar, et al., "Developing a fluorescent hybrid nanobiosensor based on quantum dots and azoreductase enzyme formethyl red monitoring", *Iranian Biomedical Journal 25*(1), 2021.

[23] M. Shirayama et al., "Degradation mechanism of $CH_3NH_3PbI_3$ perovskite materials upon exposure to humid air," Journal of

Applied Physics, vol. 119, no. 11, p. 115501, Mar. 2016, doi: 10.1063/1.4943638.

[24]E. Al-Oubidy and F. Kadhim, “Photocatalytic activity of anatase titanium dioxide nanostructures prepared by reactive magnetron sputtering technique,” Optical and Quantum Electronics, vol. 51, Jan. 2019, doi: 10.1007/s11082-018-1738-z.

[25]“Titanium dioxide (anatase).” https://webbook.nist.gov/cgi/cbook. (Accessed Sep. 06, 2022).

[26]A. M. Alturki, Department of Chemistry, Faculty of Science, University of Tabuk, Saudi Arabia;, R. Ayad, and Department of Physics, Faculty of Science, University of Tabuk, Saudi Arabia;, “Synthesis and Characterization of Titanium Dioxide Nanoparticles with a Dosimetry Study of their Ability to Enhance Radiation Therapy using a Low Energy X-ray Source,” Indian Journal of Science and Technology, vol. 12, no. 9, pp. 1–5, Mar. 2019, doi: 10.17485/ijst/2019/v12i9/140977.

[27]S. Myat, T. Htay, S. N. Khine and K. P. P. Tun, “XRD and SEM Analysis, and Semiconductor Type Determination of TiO_2 for Dye-sensitized Solar Cell,” vol. 4, no. 2.

[28]Yu *et al.*, “Ultrasmooth Perovskite Film via Mixed Anti-Solvent Strategy with Improved Efficiency,” *ACS Appl. Mater. Interfaces*, p. 11, 2017.

[29]M. K. Tariq et al., “Comparative study of Ag, Sn or Zn doped TiO_2 thin films for photocatalytic degradation of methylene blue and methyl orange,” Mater. Res. Express, vol. 6, no. 10, p. 106435, Sep. 2019, doi: 10.1088/2053-1591/ab3efd.

[30]R. S. Dubey, S. R. Jadkar, and A. B. Bhorde, “Synthesis and Characterization of Various Doped TiO_2 Nanocrystals for Dye-Sensitized Solar Cells,” ACS Omega, vol. 6, no. 5, pp. 3470–3482, Feb. 2021, doi: 10.1021/acsomega.0c01614.

[31]M. M. Karkare, “Estimation of band gap and particle size of TiO_2 nanoparticle synthesized using sol-gel technique,” in 2014 International Conference on Advances in Communication and Computing Technologies (ICACACT 2014), Aug. 2014, pp. 1–5. doi: 10.1109/EIC.2015.7230747.

[32]T. Moore and B. Bartlett, “Lowering the Band Gap of Anatase-Structured TiO_2 by Coalloying with Nb and N: Electronic Structure and Photocatalytic Degradation of Methylene Blue Dye,” The Journal of Physical Chemistry C, vol. 116, pp. 5986–5994, Feb. 2012, doi: 10.1021/jp2078456.

[33]X. Liu, Z. Wu, Y. Zhang, and C. Tsamis, “Low temperature Zn-doped TiO_2 as electron transport layer for 19% efficient planar perovskite solar cells,” Applied Surface Science, vol. 471, pp. 28–35, Mar. 2019, doi: 10.1016/j.apsusc.2018.11.237.

[34]M. I. Khan *et al.*, “300 keV cobalt ions irradiations effect on the structural, morphological, optical and photovolatic properties of Zn doped TiO_2 thin films based dye-sensitized solar cells,” *Ceramics International*, vol. 46, Mar. 2020, doi: 10.1016/j.ceramint.2020.03.256.

[35]B. Ünlü, S. Çakar, and M. Özacar, “The effects of metal-doped TiO_2 and dithizone-metal complexes on DSSCs performance,” *Solar Energy*, vol. 166, pp. 441–449, May 2018, doi: 10.1016/j.solener.2018.03.064.

[36]Xiaotao Liu, Zhenhua Wu, Yiqiang Zhang, and Christos Tsamis. Low temperature zn-doped TiO_2 as electron transport layer for 19% efficient planar perovskite solar cells. Applied Surface Science, 471:28–35, 2019.

[37]Weiguang Kong, Zhenyu Ye, Zhen Qi, Bingpo Zhang, Miao Wang, Arash Rahimi-Iman, and Huizhen Wu. Characterization of an abnormal photoluminescence behavior upon crystal-phase transition of perovskite $CH_3NH_3PbI_3$. Physical Chemistry Chemical Physics, 17(25):16405–16411, 2015.

[38]Yasuhiro Yamada, Toru Nakamura, Masaru Endo, Atsushi Wakamiya, and Yoshihiko Kanemitsu. Near-band-edge optical responses of solution-processed organic–inorganic hybrid perovskite ch3nh3pbi3 on mesoporous tio2 electrodes. Applied Physics Express, 7(3):032302, 2014.

[39]A. Baktash, O. Amiri, and A. Sasani, “Improve efficiency of perovskite solar cells by using Magnesium doped ZnO and TiO_2 compact layers,” *Superlattices and Microstructures*, vol. 93, pp. 128–137, May 2016, doi: 10.1016/j.spmi.2016.01.026.